Contents lists available at ScienceDirect

Digital Chinese Medicine

journal homepage: http://www.keaipublishing.com/dcmed

Integrated network pharmacology and experimental validation for identification of mechanism of icariin targeting PLK1 in inhibiting hepatocellular carcinoma

Wei Zhang[a], Fenglian Ma[a], Xiangjun Sun[b*]

a. Linyi People's Hospital Graduate Training Base, Guangzhou University of Chinese Medicine, Linyi, Shandong 276003, China

b. Department of Hepatobiliary Surgery, Linyi People's Hospital, Linyi, Shandong 276003, China

ARTICLE INFO

Article history
Received 25 June 2025
Accepted 24 December 2025
Available online 25 March 2026

Keywords
Icariin
Hepatocellular carcinoma
Polo-like kinase 1 (PLK1)
Phosphorylation
Molecular docking

ABSTRACT

Objective To systematically elucidate the molecular mechanisms and core targets underlying the anti-hepatocellular carcinoma (HCC) effects of icariin through integrated network pharmacology and experimental validation.

Methods Potential targets of icariin were screened using the PubChem database and SwissTargetPrediction platform, followed by intersection analysis with HCC-related genes from the Cancer Genome Atlas (TCGA) and Gene Expression Omnibus (GEO). Gene Ontology (GO) enrichment and Kyoto Encyclopedia of Genes and Genomes (KEGG) pathway analyses were performed to characterize the biological functions of candidate targets. Key genes were identified using the random survival forest algorithm, and their associations with the tumor microenvironment were evaluated through immune infiltration analysis. Molecular docking was employed to predict the binding affinity between icariin and its core targets, which was subsequently validated by *in vitro* enzyme inhibition assays. Functional targets were determined through overexpression experiments in HepG2 cells, and mechanistic investigations were conducted using Western blot and co-immunoprecipitation techniques. *In vivo* anti-tumor efficacy was evaluated using a subcutaneous HepG2 xenograft mouse model by monitoring tumor volume progression and endpoint tumor weight, and the impact of polo-like kinase 1 (PLK1) overexpression on icariin-mediated tumor growth inhibition was assessed.

Results Network pharmacology analysis identified 36 common targets between icariin and HCC, which were primarily enriched in hypoxia-inducible factor-1 (HIF-1), phosphatidylinositol 3-kinase/protein kinase B (PI3K/AKT), and forkhead box O (FoxO) signaling pathways. Among these, *PLK1*, ATP binding cassette subfamily C member 1 (*ABCC1*), and matrix metallopeptidase 3 (*MMP3*) were identified as key genes, with their high expression significantly associated with poor patient prognosis ($P < 0.000\,1$, $P = 0.004$, and $P = 0.03$, respectively). Immune infiltration analysis revealed significant correlations between these three genes and various immune cell types, suggesting their involvement in modulating the tumor immune microenvironment. Molecular docking predicted stable binding between icariin and these targets, and *in vitro* enzymatic assays confirmed that icariin (20 μmol/L) exhibited the highest inhibitory rate against PLK1 (49.67% ± 4.19%), significantly greater than that against ABCC1 (24.33% ± 3.40%) and MMP3 (38.00% ± 3.06%). Functional validation demonstrated that PLK1 overexpression reversed icariin-mediated inhibition of HepG2 cell proliferation

*Corresponding author: Xiangjun Sun, E-mail: sunxjun2004@sina.com.

Peer review under the responsibility of Hunan University of Chinese Medicine.

DOI: 10.1016/j.dcmed.2026.02.012

Citation: ZHANG W, MA FL, SUN XJ. Integrated network pharmacology and experimental validation for identification of mechanism of icariin targeting PLK1 in inhibiting hepatocellular carcinoma. Digital Chinese Medicine, 2026, 9(1): 130-143.

($P < 0.05$), whereas ABCC1 or MMP3 overexpression showed no such effect, indicating PLK1 as the primary functional target of icariin. Mechanistic studies revealed that icariin specifically reduced PLK1 phosphorylation levels and disrupted its interaction with forkhead box M1 (FoxM1). *In vivo* experiments confirmed that PLK1 overexpression significantly attenuated icariin-induced suppression of tumor growth in xenograft mice ($P < 0.001$).

Conclusion PLK1 is a critical target mediating the anti-HCC effects of icariin through inhibition of the PLK1-FoxM1 axis, providing a mechanistic basis for the clinical development of icariin as an HCC therapeutic agent.

1 Introduction

Hepatocellular carcinoma (HCC) represents a major global health burden, with limited effective therapeutic strategies. In China, HCC poses a particularly severe health challenge, accounting for approximately 366 000 new cases and 318 000 deaths annually, ranking as the fourth most common malignancy and the second leading cause of cancer-related mortality [1]. Existing effective therapies, including surgical resection, transcatheter arterial chemoembolization, and systemic chemotherapy, are constrained by poor curative efficacy, suboptimal patient tolerance, and significant side effects, particularly in patients with underlying liver dysfunction [2].

Naturally derived compounds from traditional Chinese medicine (TCM) represent a compelling avenue for anticancer drug discovery. Yinyanghuo (Epimedii Folium), a well-established medicinal herb, has garnered considerable interest for its multifaceted pharmacological properties, including immunomodulatory and antitumor activities [3]. Icariin, the principal bioactive flavonoid component of Yinyanghuo (Epimedii Folium), exhibits low toxicity and potent anticancer activity across diverse malignancies, such as non-small cell lung cancer, breast cancer, and gastric cancer [4-7]. Critically, beyond its documented effects of inhibiting proliferation and inducing apoptosis in HCC cells, icariin has shown promise in modulating key oncogenic pathways, such as phosphatidylinositol-3-kinase/protein kinase B (PI3K/AKT) and Wnt/β-catenin [6]. This multi-target profile positions it as a potential candidate for addressing the key challenge of limited efficacy and acquired resistance associated with single-target therapies in HCC [6].

However, despite these preclinical findings, the precise molecular mechanisms underlying icariin's anti-HCC effects remain incompletely understood. This knowledge deficit poses a substantial barrier to its clinical translation and rational development as a targeted therapeutic agent. The emergence of network pharmacology provides a powerful framework to address this limitation, by enabling systematic identification of drug-target interactions and comprehensive analysis of underlying pharmacological mechanisms, which is particularly well-suited for studying multi-target natural products like icariin [8].

Therefore, this study aims to integrate network pharmacology with experimental validation to elucidate the mechanism underlying the icariin-mediated anti-HCC effects. We hypothesize that icariin exerts its therapeutic effects through the specific targeting of key molecules involved in HCC progression. Through bioinformatics analysis of public databases combined with rigorous *in vitro* and *in vivo* validation, we aim to identify the molecular targets of icariin and provide new insights into the development of icariin-based treatment strategies for HCC.

2 Materials and methods

2.1 Icariin targets screening

The icariin target swere systematically screened using the PubChem database (Compound Identifier: 5318997) [9] and SwissTargetPrediction platform (https://www.swisstargetprediction.ch; based on molecular similarity and pharmacophore models) [10]. Potential targets were selected with a probability threshold > 0.1. Pathological targets associated with HCC were retrieved from the following sources: the Online Mendelian Inheritance in Man (OMIM) database using "hepatocellular carcinoma" as the search term [11]; the GeneCards database with the same search term and a relevance score threshold of ⩾ 10 [12]; and the Gene Expression Omnibus (GEO) database, from which disease-related targets were identified based on differential expression analysis of HCC-related datasets [13]. The GEO datasets (accession number: GSE112271) involved in this study contained mRNA expression profiles of HCC tissues and adjacent non-tumor tissues. To elucidate the potential mechanisms of TCM against HCC, icariin targets, and HCC-related pathological targets were integrated with Venn diagrams in the R package "VennDiagram" [14]. The overlapping targets from the integration were considered as the potential icariin targets for HCC treatment.

2.2 HCC datasets

HCC data were obtained from the Cancer Genome Atlas (TCGA) and GEO, and the comprehensive molecular profiling and clinical annotations were provided by these two databases. Specifically, a total of 424 TCGA samples (50 normal and 374 tumor) with full mRNA sequencing data

and clinical annotations were incorporated. For GSE112271, seven tumor samples meeting stringent quality thresholds were enrolled for data integrity and cell type annotations to ensure robust tumor microenvironment analysis [15].

2.3 Gene Ontology (GO) analysis and Kyoto Encyclopedia of Genes and Genomes (KEGG) function analysis

Functional annotation of the overlapping targets between icariin and HCC was performed using the R package "clusterProfiler" for GO analysis and KEGG pathway enrichment analysis. The significance threshold was set at a false discovery rate (FDR)-adjusted $P < 0.05$.

2.4 Random survival forest (RSF) algorithm

The RSF algorithm was implemented with the random ForestSRC package to screen the feature genes from the overlapping targets between icariin and HCC. These genes related to prognosis were ranked using the RSF algorithm (nrep = 1 000, indicating that the number of iterations in the Monte Carlo simulation was 1 000). Genes with a relative importance > 0.3 were identified as key genes.

2.5 Immune cell infiltration analysis

The Characterizing Immune Cell Basis Expression Reference SORTing (CIBERSORT) algorithm using gene expression data was applied using the LM22 signature matrix for the HCC patient data and relative proportions of 22 immune-infiltrating cells [16]. Spearman's correlation analysis was performed to assess the correlations between gene expression and immune cell content, and $P < 0.05$ was considered statistically significant.

2.6 Gene set enrichment analysis (GSEA) and gene set variation analysis (GSVA)

Further analysis of the signaling pathway differences between the high- and low-expression groups of the key genes for the specific targets were performed using GSEA. The background gene set was obtained from the Molecular Signatures Database (MSigDB) 7.0 [17] and annotated gene sets were employed as subtype pathways. Differential expression analysis of pathways between subtypes was performed, and significantly enriched gene sets (adjusted P value < 0.05) were ranked according to their enrichment scores. The GSVA algorithm was employed to assign comprehensive scores for each gene set and evaluate potential biological function changes across various samples.

2.7 Regulatory network analysis of key genes

Transcription factor prediction for the key genes was performed using the R package "RcisTarget" based on motif enrichment analysis. All computations utilized the "rcistarget.hg19.motifdb.cisbpont.500bp" gene-motif rankings database. The analysis procedure involved the area under the recovery curve for each motif-gene set pair, with the normalized enrichment score derived from the area under the curve distribution across all motifs. Beyond the originally annotated motifs, additional annotations were inferred through motif similarity and gene sequence analysis. These motifs were identified with the database-recommended thresholds of normalized enrichment score > 3.0 and FDR < 0.05 [18].

2.8 miRNA-mRNA network construction

To construct the miRNA-mRNA regulatory network, the miRNA-target interactions for the key genes from the miRcode database (V11) were first retrieved and experimentally validated [19]. All interactions provided by the database with a default confidence level were included. The resulting interaction pairs were then imported into Cytoscape software (V3.9.1) [20] for network visualization and analysis. In the generated network, nodes represented miRNAs or mRNAs, and edges represented predicted regulatory relationships. The network layout was optimized for clarity using the built-in Cytoscape layout algorithms.

2.9 Molecular docking

The key target proteins were obtained from the Protein Data Bank (PDB; https://www.rcsb.org/) for known structures and unavailable structures were predicted using AlphaFold 3. The molecular structure of icariin was retrieved from the PubChem database (https://pubchem.ncbi.nlm.nih.gov). Protein structures were prepared through water molecule removal, addition of hydrogen atoms, and assignment of partial charges using PyMOL (V2.5.4). Icariin was energy-minimized using the Merck Molecular Force Field (MMFF94). Molecular docking was performed using AutoDock (V4.2.6) with the Lamarckian Genetic Algorithm. The grid box dimensions were set to 40 × 40 × 40 Å with 0.375 Å spacing, centered on the known active site of each protein. Docking poses were evaluated by binding energy, with complexes exhibiting binding energies < 0 kcal/mol considered indicative of binding between the ligands and receptors [21]. The most favorable binding conformation for each target was selected for further analysis based on both binding energy values and cluster analysis.

2.10 *In vitro* inhibitory activities of icariin against the key genes

To validate the three key genes [polo-like kinase 1 (*PLK1*), ATP binding cassette subfamily C member 1 (*ABCC1*),

and matrix metallopeptidase 3 (*MMP3*)] identified through network pharmacology analysis as functional targets of icariin, *in vitro* enzymatic inhibition assays were performed. ADP-Glo™ PLK1 kinase enzyme system (Promega, USA) was used to determine PLK1 activity. Calcein AM assay was performed to determine ABCC1 activity [22]. MMP3 inhibitor screening assay kit (Abcam, UK) was employed to determine MMP3 activity. The inhibitory activity of icariin was assessed at two concentrations (10 and 20 μmol/L) across three protein activity assay systems: PLK1, ABCC1, and MMP3. The selected concentrations were based on documented recommendations [22, 23]. An equivalent volume of phosphate-buffered saline (PBS) served as the negative control group. The inhibitory effects of icariin at specific concentrations were assessed by calculating the ratio of protein activity in the icariin-treated groups to that of the negative control group.

2.11 Cell culture

Wild-type (WT) HepG2 cells were obtained from the American Type Culture Collection (ATCC, USA). Stable PLK1-overexpressing HepG2 cells (sPLK1-OV) were established through lentiviral transduction using the pCDH-CMV-MCS-EF1-Puro vector (System Biosciences, USA) containing the full-length human PLK1 cDNA sequence. Following transduction, cells underwent selection with 2 μg/mL puromycin (Thermo Fisher Scientific, USA) for 14 d. Successful PLK1 overexpression was confirmed at both protein and mRNA levels through Western blot and quantitative reverse transcription polymerase chain reaction (qRT-PCR) analysis, respectively.

All HepG2 cell lines were maintained in Dulbecco's Modified Eagle Medium (DMEM, Thermo Fisher Scientific, USA) supplemented with 10% fetal bovine serum (FBS, GIBCO, USA) and 1% penicillin-streptomycin (Thermo Fisher Scientific, USA). Cells were cultured at 37 °C in a humidified atmosphere containing 5% CO_2. Regular subculturing was performed every 3 – 4 d using 0.25% trypsin-ethylenediaminetetraacetic acid (EDTA) (Thermo Fisher Scientific, USA) upon reaching 80% – 90% confluence.

2.12 Cell transfection

PLK1-, ABCC1-, or MMP3- overexpressing plasmids (named iPLK1-OV HepG2, iABCC1-OV HepG2, and iMMP3-OV HepG2, respectively) were constructed by Fitgene (Guangzhou, China) and transiently transfected into HepG2 cells using Lipofectamine 3000. Forkhead box M1 (FoxM1) siRNA was purchased from Thermo Fisher Scientific and transiently transfected into HepG2 cells simultaneously with PLK1- overexpressing plasmid (named iPLK1-OV-FoxM1-KD HepG2) using Lipofectamine 3000.

2.13 Cell counting kit-8 (CCK-8) assay

After 24 h of adhesion, cells were collected and inoculated at a density of 1×10^3 cells/well in 96-well plates, with blank controls (medium without cells) included on each plate. After 24 h of adhesion, cells were treated according to the respective experimental groups (e.g., vehicle control, icariin at various concentrations, and transfected cell lines). The specific composition of each group is detailed in the corresponding results section for each experiment. Following 48 h of treatment, cell viability was measured using the CCK-8 kit (Dojindo, Japan) according to the manufacturer's instructions, with absorbance recorded at 450 nm using a microplate reader. Cell viability was calculated using the following formula: viability (%) = [(A_treatment – A_blank)/(A_vehicle control – A_blank)] × 100%.

For experiments comparing drug responses across genetically modified cell lines (e.g., PLK1-OV), data were further normalized to isolate the drug-specific effect. For each distinct cell line (e.g., WT, PLK1-OV), the viability of its vehicle control group (0 μg/mL icariin) was defined as the baseline control (set to 100%). The viability of its corresponding drug-treated group was then expressed as a percentage relative to this internal baseline using the formula: normalized viability (%) = (viability_treatment/viability_vehicle control) × 100%. This baseline normalization allows for the direct comparison of icariin's inhibitory efficacy independent of the inherent proliferation differences among the cell lines.

2.14 Western blot and co-immunoprecipitation (Co-IP) assays

Western blot and Co-IP assays were performed to evaluate the expression and phosphorylation of PLK1 and to examine the interaction between PLK1 and FoxM1 [24]. For Co-IP, whole-cell lysates were incubated with anti-PLK1 antibody (Abcam, UK) overnight at 4 °C, followed by incubation with protein A/G agarose beads (Thermo Fisher Scientific, USA). Normal rabbit IgG (Abcam, UK) served as the negative control. For Western blot, proteins were transferred to polyvinylidene fluoride (PVDF) membranes (Merck, Germany) after electrophoresis and blocked with 5% non-fat milk. Membranes were incubated with primary antibodies against PLK1 (Abcam, UK), phosphorylation-PLK1 (p-PLK1, Abcam, UK), FoxM1 (Abcam, UK), and glyceraldehyde-3-phosphate dehydrogenase (GAPDH) (Abcam, UK) overnight at 4 °C, followed by incubation with horseradish peroxidase (HRP)-conjugated secondary antibodies (Abcam, UK) for 1 h at room temperature.

2.15 Reverse transcription quantitative polymerase chain reaction (RT-qPCR) analysis

Total RNA was extracted from cultured cells using TRIzol reagent and treated with DNase I to remove genomic

DNA. cDNA was synthesized from 1 μg of total RNA using a reverse transcription kit (PrimeScript™ RT reagent kit). RT-qPCR was performed on a Bio-Rad CFX96 real-time PCR system using SYBR Green chemistry. Each reaction mixture contained cDNA template, gene-specific primers, and SYBR Green master mix. The primer sequences were as follows: GAPDH (forward, 5'-TGTGGGCATCAATGGATTTGG-3'; reverse, 5'-ACACCATGTATTCCGGGTCAAT-3'), PLK1 (forward, 5'-CAGTCACTCTCCGCGACAC-3'; reverse, 5'-GAGTAGCCGAATTGCTGCTG-3'), ABCC1 (forward, 5'-GTGAATCGTGGCATCGACATA-3'; reverse, 5'-GCTTGGGACGGAAGGGAATC-3'), MMP3 (forward, 5'-AGTCTTCCAATCCTACTGTTGCT-3'; reverse, 5'-TCCCCGTCACCTCCAATCC-3'). The amplification conditions were as follows: initial denaturation at 95 °C for 30 s, followed by 40 cycles of denaturation at 95 °C for 5 s and annealing/extension at 60 °C for 30 s. Relative gene expression levels were calculated using the $2^{-\Delta\Delta Ct}$ method, with GAPDH as the internal reference.

2.16 *In vivo* xenograft model and icariin treatment

A total of 24 specific pathogen-free (SPF) grade female BALB/c nude mice (6 – 8 weeks old, 18 – 22 g) were obtained from Beijing Vital River Laboratory Animal Technology Co., Ltd. (Charles River, China). All animals were acclimatized for 7 prior to experimentation and maintained under SPF conditions with controlled environmental parameters: temperature of 22 ± 2 °C, humidity of 55% ± 10%, a 12-h light/dark cycle, and free access to food and water. All animal experiments were conducted in the animal facility of Beijing Langke Biotechnology Co., Ltd. The experimental protocol was approved by the Institutional Animal Care and Use Committee (IACUC) of Beijing Langke Biotechnology Co., Ltd. [Animal Ethics Approval No. IACUC-20230901-01; Facility License No. SYXK (Jing) 2023-0004; Laboratory Animal Use License No. 110324231104736913].

A subcutaneous xenograft model was generated by injecting 2 × 10^6 WT or sPLK1-OV HepG2 cells into the flanks of 24 female BALB/c nu/nu mice (6 – 8 weeks old). Mice were randomly allocated into four groups (n = 6 per group): WT + vehicle, WT + icariin [40 (mg/kg·d)], sPLK1-OV + vehicle, and sPLK1-OV + icariin [40 (mg/kg·d)]. The vehicle consisted of normal saline containing 0.5% carboxymethylcellulose sodium (CMC-Na), and the icariin dose was selected based on prior effective dosing reported in reference [25]. Treatment was initiated when tumors reached approximately 100 mm^3 (defined as day 0). Tumor volumes were measured every 3 – 4 d, and volume was calculated using the formula: volume = 0.5 × length × $width^2$. Sample size was determined based on preliminary data, to detect a 30% difference in tumor volume with 80% power at α = 0.05. Mice were excluded from analysis if tumor implantation failed (no palpable tumor within 14 d after cell injection), body weight loss exceeded 15% compared with the weight at the start of treatment, injection-site infection occurred, or intercurrent illness developed.

2.17 Statistical analysis

All statistical analyses were performed using R language (V4.3.0). Data are presented as mean ± standard deviation (SD). For comparisons between two groups, Student's t test was employed, while one-way analysis of variance (ANOVA) with appropriate post-hoc testing was applied for comparisons among groups. Two-way ANOVA was performed to compare multiple mean values across conditions. $P < 0.05$ was considered statistically significant.

3 Results

3.1 Network pharmacology elucidation of potential targets of icariin in HCC

Using the PubChem and SwissTargetPrediction databases, a total of 84 icariin-target proteins were identified (Figure 1A). Concurrently, 1 711 HCC-related disease targets were retrieved from the GeneCards and OMIM databases. Intersection analysis of the 84 drug targets with the 1 711 disease targets yielded 36 common targets (Figure 1B), which were considered putative key mediators underlying the therapeutic action of icariin against HCC. GO enrichment analysis of these 36 overlapping targets, performed using the ClusterProfiler R package, indicated predominant associations with cellular responses to chemical stress, oxidative stress, and circadian rhythm processes (Figure 1C). KEGG pathway enrichment further revealed significant involvement in the hypoxia-inducible factor-1 (HIF-1), phosphatidylinositol 3-kinase/protein kinase B (PI3K/AKT), and forkhead box O (FoxO) signaling pathways (Figure 1D). To illustrate the integrative relationships among icariin, its predicted targets, and related pathways, a comprehensive network diagram was constructed with Cytoscape (Figure 1E).

To further identify key genes among the 36 intersecting target genes, the RSF analysis was conducted. Genes with a relative importance > 0.3 were determined as key genes (Figure 2A). The *PLK1*, *ABCC1*, and *MMP3* genes were identified (Figure 2B). Additionally, survival analysis of the three genes revealed statistically significant differences in survival between the PLK1 high- and low-expression groups ($P < 0.000\,1$, Figure 2C), the ABCC1 high- and low-expression groups ($P = 0.004$, Figure 2D), and the MMP3 high- and low-expression groups ($P = 0.03$, Figure 2E). Based on these results, PLK1, ABCC1, and MMP3 were prioritized as potential therapeutic targets for icariin.

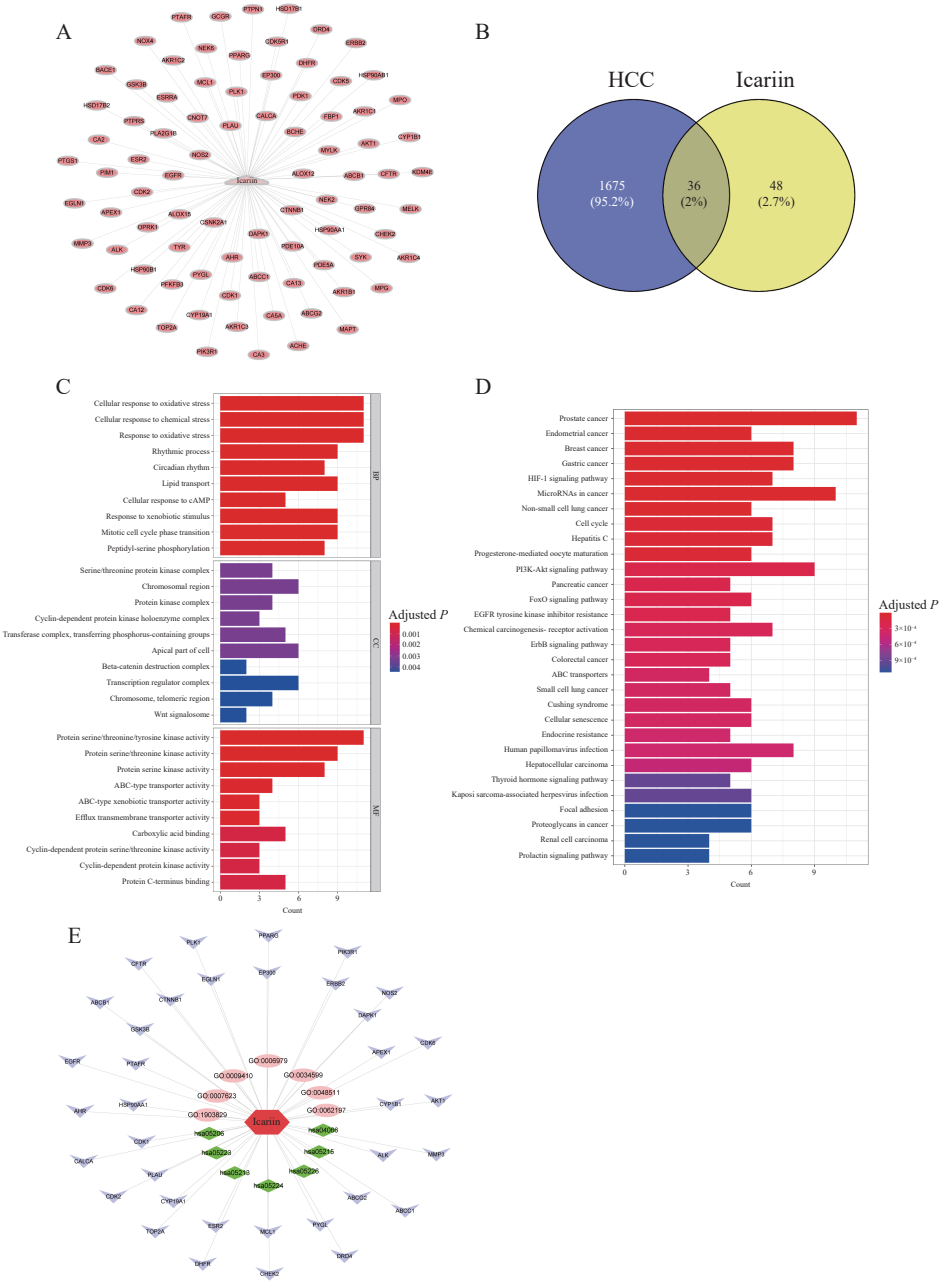

Figure 1 Identification and functional enrichment of icariin targets in HCC

A, Cytoscape network of icariin and its targets. B, overlap of icariin and HCC co-targets. C, GO enrichment analysis of target genes. D, KEGG pathway enrichment analysis of target genes. E, Cytoscape network of icariin, pathways, and intersecting genes. Icariin is flanked by an inner ring of enriched pathways (GO, pink; KEGG, green) and an outer ring of target genes.

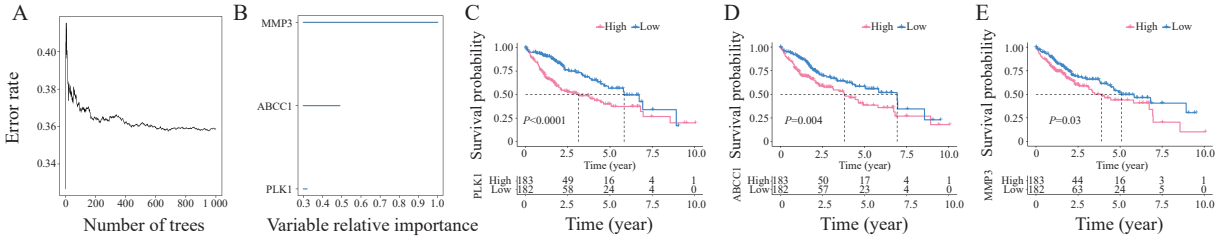

Figure 2 RFS analysis of the target genes on HCC patients

A, ranking of feature genes by random survival forest. B, identification of *PLK1*, *ABCC1*, and *MMP3* as key genes. C – E, survival analysis of three key genes (*PLK1*, *ABCC1*, and *MMP3*, respectively).

3.2 Correlation analysis between key genes and immune infiltration in HCC

To systematically evaluate the immunomodulatory function of the key targets of icariin, we further analyzed the correlations between PLK1, ABCC1, MMP3 and the immune infiltration in HCC. The infiltration levels of immune cells in HCC tissues were quantified using the CIBERSORT algorithm (Figure 3A). Macrophages accounted for relatively high proportions in both normal and tumor samples. Significant differences in certain immune cell subtypes were observed between normal and tumor tissues (P < 0.001); for instance, naïve B cells showed lower infiltration levels in tumor samples compared with normal samples. A correlation network among the immune cells was constructed (Figure 3B), with red lines indicating potential positive regulatory relationships, such as the strong positive correlation observed between naïve CD4+ T cells and resting mast cells. Compared with adjacent tissues, HCC tissues exhibited a significant imbalance in immune cell proportions, with marked increases in regulatory T cells, M0 macrophages, resting dendritic cells and mast cells (P < 0.001, Figure 3C).

Correlation analysis between key targets and immune characteristics revealed that high PLK1 expression was significantly associated with increased infiltration of follicular helper T cells and M0 macrophages, while showing negative correlations with resting memory CD4+ T cells and monocytes (P < 0.05, Figure 3D). ABCC1 expression positively correlated with M0 macrophages and

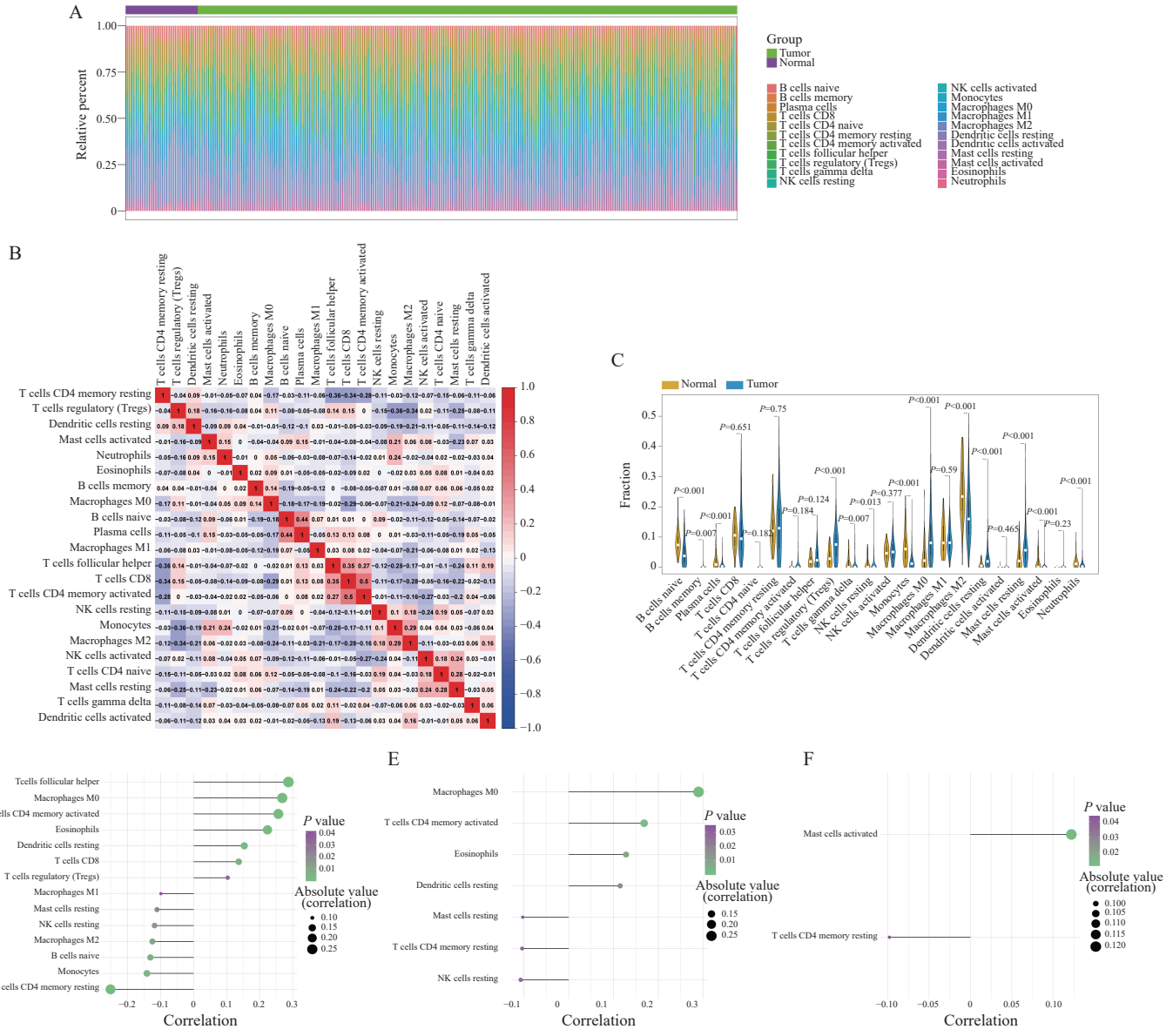

Figure 3 Immune infiltration analysis of key genes in HCC tissues

A, relative proportions of 22 immune cell types in HCC tissues. B, Pearson correlation among immune cell types (blue: negative, red: positive). C, immune cell differences between control and HCC samples. D – F, correlations between immune cell infiltration and PLK1, ABCC1, and MMP3, respectively.

activated memory CD4+ T cells, but negatively with resting NK cells andmemory CD4+ T cells ($P < 0.05$, Figure 3E). MMP3 demonstrated positive correlation with activated mast cells and negative correlation with resting memory CD4+ T cells ($P < 0.05$, Figure 3F). These findings indicated a regulatory correlation between icariin's targets and the immune microenvironment, suggesting a potential immunomodulatory mechanism in its anti-HCC activity.

Subsequently, correlations of PLK1, ABCC1, and MMP3 with various immune related factors were analyzed, including chemokines [Figure 4A; e.g., C-X-C motif chemokine ligand 3 (CXCL3) showed a positive correlation with all three targets, whereas C-C motif chemokine ligand 14 (CCL14) was negatively correlated with them], immunoinhibitors [Figure 4B; e.g., galectin-9 (LGALS9) was positively correlated with all three targets, while adenosine Aza receptor (ADORA2A) correlated negatively with PLK1 and ABCC1 but positively with MMP3], immunostimulators [Figure 4C; e.g., tumor necrosis factor receptor superfamily member 8 (TNFRSF8) correlated positively with all three targets, whereas interleukin-6 receptor (IL6R) correlated negatively with ABCC1], MHC molecules [Figure 4D; e.g., C-X-C motif chemokine ligand 4 (CXCR4) showed positive correlation with all three targets], and immune receptors [Figure 4E; e.g., transporter associated with antigen processing 1 (TAP1) correlated positively with all three targets). The strong associations of PLK1, ABCC1, and MMP3 with immune cell infiltration suggest that these targets may mediate the regulatory effects of icariin on the tumor immune microenvironment.

3.3 Pathway enrichment analysis of PLK1, ABCC1, and MMP3 in HCC

The specific signaling pathways associated with PLK1, ABCC1, and MMP3 were investigated to explore the potential molecular mechanisms by which these key genes may affect the HCC progression. GSEA indicated that PLK1 was significantly enriched in the Fanconi anemia pathway, mRNA surveillance pathway, and Notch signaling pathway (Figure 5A and 5B). GSVA further demonstrated its enrichment in the phosphatidylinositol 3-kinase–protein kinase B–mechanistic target of rapamycin (PI3K-AKT-mTOR) signaling pathway, apoptosis, and the p53 signaling pathway (Figure 5C). For ABCC1, GSEA showed enrichment in the Fc epsilon RI signaling pathway, vascular endothelial growth factor (VEGF) signaling pathway,andtumornecrosisfactor(TNF)signalingpathway (Figure 5D and 5E). GSVA analysis revealed its association with the interleukin-2-signal transducer and activator of transcription 5 (IL-2-STAT5) signaling pathway, PI3K-AKT-mTOR signaling pathway, and Wnt/β-catenin signaling pathway (Figure 5F). Regarding MMP3, GSEA results identified enrichment in the cytosolic DNA-sensing pathway, nucleotide-binding oligomerization domain (NOD)-like receptor signaling pathway, and IL-17 signaling pathway (Figure 5G and 5H). Corresponding GSVA confirmed its enrichment in the p53 signaling pathway, interleukin-6-Janus kinase-signal transducer and activator of transcription 3 (IL-6-JAK-STAT3) signaling pathway, and reactive oxygen species (ROS) pathway (all $P < 0.0001$; Figure 5I).

3.4 *In vitro* validation of icariin targets

To further validate the therapeutic relevance of PLK1, ABCC1, and MMP3 as novel antitumor targets of icariin, we employed an integrated approach combining molecular docking simulations with experimental validation. Molecular docking analysis revealed that icariin formed energetically favorable complexes with all three targets, as evidenced by negative binding free energy values for PLK1 (Figure 6A, – 2.32 kcal/mol), ABCC1 (Figure 6B, – 2.94 kcal/mol), and MMP3 (Figure 6C, – 2.96 kcal/mol), suggesting stable binding interactions.

To evaluate the *in vitro* inhibitory activity of icariin against PLK1, ABCC1, and MMP3, kinase and enzyme assays were performed. As shown in Figure 6D, icariin at concentrations of 10 and 20 μmol/L significantly suppressed enzyme activities: PLK1 activity was reduced by 32.67% ± 3.06% ($P < 0.001$) and 49.67% ± 4.19% ($P < 0.001$), ABCC1 by 18.33% ± 1.53% ($P < 0.001$) and 24.33% ± 3.40% ($P < 0.001$), and MMP3 by 30.33% ± 3.06% ($P < 0.001$) and 38.00% ± 3.61% ($P < 0.001$), respectively. Minimal inhibition was observed in the negative control group, confirming the *in vitro* targeting specificity of icariin toward PLK1, ABCC1, and MMP3. Subsequently, HepG2 cells were treated with icariin at different concentrations for 72 h. Icariin exerted a dose-dependent reduction in cell viability, with the IC_{50} value of approximately 100 μg/mL (92.21 μmol/L, Figure 6E).

To investigate the functional role of candidate targets, HepG2 cells were transiently transfected with PLK1, ABCC1, or MMP3 overexpression plasmids to generate iPLK1-OV HepG2, iABCC1-OV HepG2, and iMMP3-OV HepG2 cell lines, respectively. Transfection efficiency was confirmed by RT-qPCR, with all comparisons showing statistically significant upregulation ($P < 0.001$; Figure 7A). Using these models, icariin treatment markedly inhibited cell proliferation in parental HepG2 cells; however, this inhibitory effect was partially abrogated in iPLK1-OV HepG2 cells ($P = 0.041 6$), whereas no significant reversal was observed in iABCC1-OV HepG2 ($P > 0.05$) or

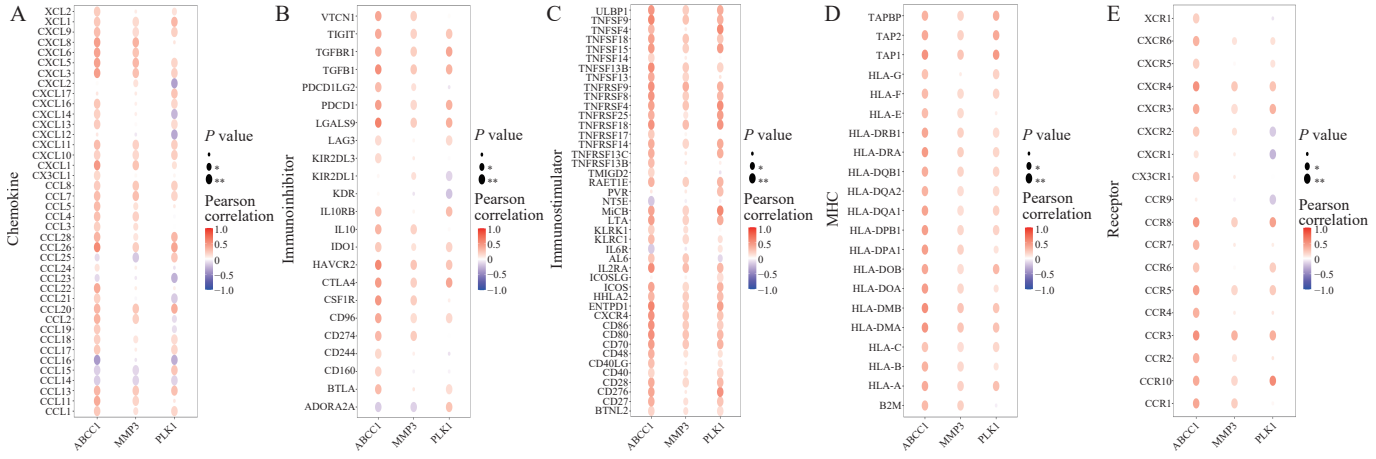

Figure 4 Correlation analysis between key genes and immune regulatory factors in HCC tissues

A – E, associations of PLK1, ABCC1, and MMP3 with chemokines, immunoinhibitors, immunostimulators, MHC, and receptors molecules, respectively. Blue indicates negative correlations and red indicates positive correlations.

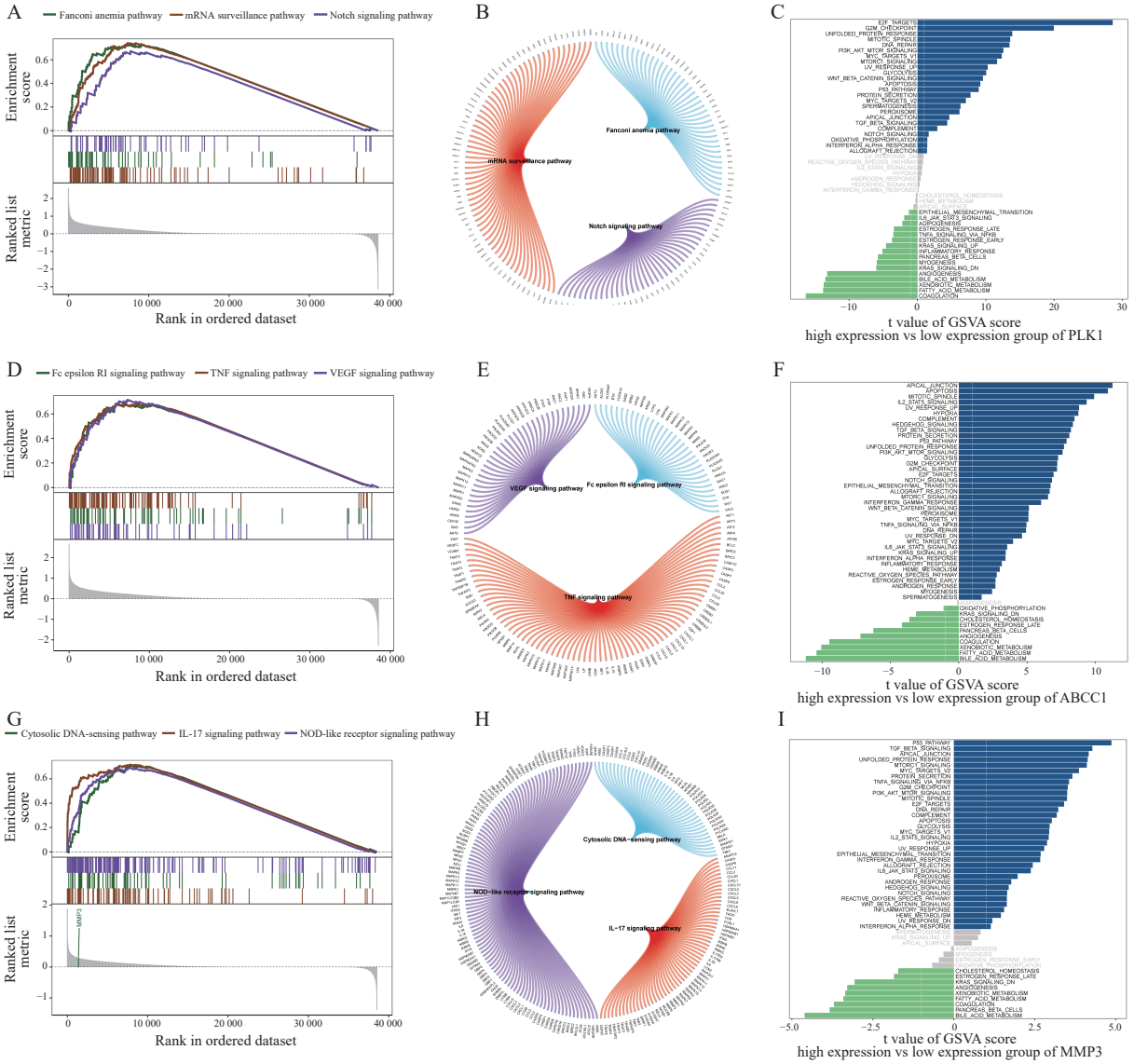

Figure 5 GSEA and GSVA analysis of key genes in HCC

A, GSEA enrichment for PLK1. B, top enriched pathways and associated genes for PLK1. C, GSVA for PLK1. D, GSEA enrichment for ABCC1. E, top enriched pathways and associated genes for ABCC1. F, GSVA for ABCC1. G, GSEA enrichment for MMP3. H, top enriched pathways and associated genes for MMP3. I, GSVA for MMP3.

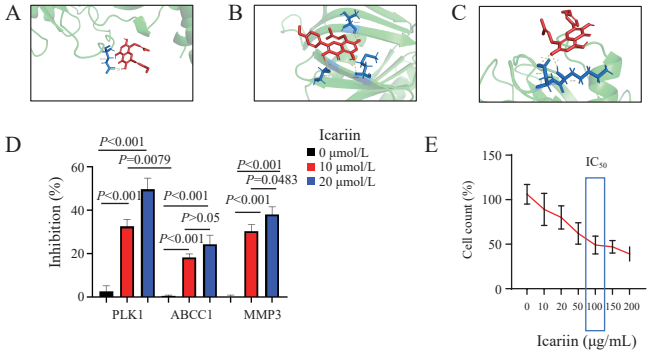

Figure 6 Validation of PLK1, ABCC1, and MMP3 as targets of icariin and its inhibitory effects on HCC cells

A – C, binding modes of icariin with PLK1, ABCC1, and MMP3, respectively. D, *in vitro* inhibition of PLK1, ABCC1, and MMP3 activities by icariin. E, viability of WT HepG2 cells assessed by CCK-8 assay after 72 h of icariin treatment.

iMMP3-OV HepG2 cells ($P > 0.05$) (Figure 7B). These findings suggest that PLK1, functionally mediates the antitumor effects of icariin against HCC, highlighting the importance of PLK1 in icariin-induced growth suppression.

Treatment with 25 and 50 μg/mL icariin reduced PLK1 phosphorylation levels in WT HepG2 cells, confirming the targeting specificity of icariin for PLK1 (Figure 7C and 7D). FoxM1 has been reported as a substrate that mediates the function of PLK1 [26], and we found that

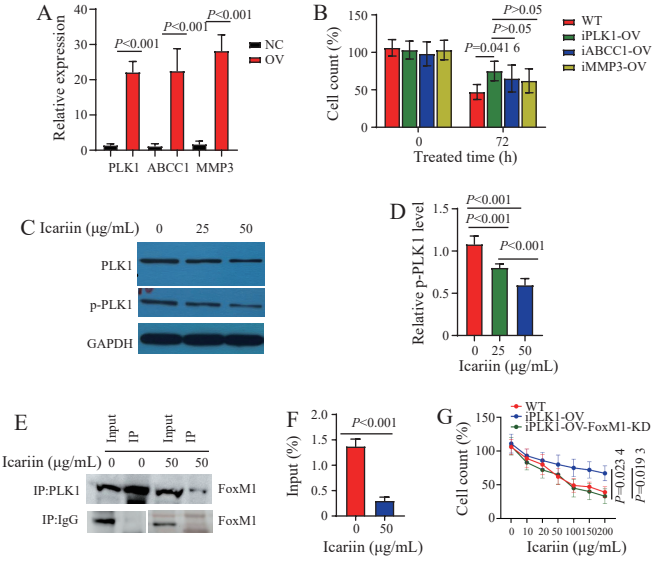

Figure 7 Validation of PLK1 as the primary novel antitumor target of icariin in HCC cells

A, transfection efficiency verified by RT-qPCR. NC, negative control (cells transfected with empty vector). OV, overexpression (cells transfected with gene-specific overexpression plasmids. B, cell viability upon icariin treatment. C, Western blot images of PLK1 and phosphorylated PLK1 (p-PLK1). D, quantification of relative P-PLK1 levels. E, Co-IP analysis of PLK1-FoxM1 interaction after icariin treatment. F, quantification of FoxM1 binding to PLK1. G, cell viability rescue by IPLK1-OV-FoxM1-KD cells.

PLK1 can bind to FoxM1, while icariin can significantly inhibit this binding ($P < 0.001$, Figure 7E and 7F). Furthermore, the anti-proliferative effect of icariin was abolished in iPLK1-OV HepG2 cells ($P = 0.0193$), indicating that icariin acts through PLK1. Notably, this effect was restored in iPLK1-OV cells upon FoxM1 knockdown (iPLK1-OV-FoxM1-KD) ($P = 0.0234$), demonstrating that PLK1 operates through FoxM1 to mediate the action of icariin (Figure 7G).

3.5 *In vivo* validation of PLK1 as a novel anti-tumor target of icariin

To evaluate the *in vivo* functions of icariin and PLK1, tumor-bearing mice were inoculated with sPLK1-OV HepG2 cells. Compared with WT + vehicle group, sPLK1-OV inoculation resulted in a marked increase in tumor burden, as illustrated by progressive elevation of tumor growth curves over time ($P < 0.001$, Figure 8A). At the experimental endpoint, macroscopic images of excised tumors revealed larger size in sPLK1-OV group relative to vehicle (Figure 8B), and quantitative analysis confirmed a significant increase in tumor weight ($P < 0.001$, Figure 8C). Administration of icariin effectively suppressed tumor growth derived from both WT HepG2 and sPLK1-OV HepG2 cells. However, the anti-tumor efficacy of icariin was notably diminished in the sPLK1-OV HepG2 group, as reflected by lower inhibitory rates on tumor volume ($P < 0.001$, Figure 8D) and tumor weight compared with the WT group ($P < 0.001$, Figure 8E). This attenuation of icariin activity *in vivo* was consistent with the corresponding *in vitro* findings. Collectively, these results indicated that icariin exerts antitumor effects both *in vitro* and *in vivo* through targeted inhibition of PLK1.

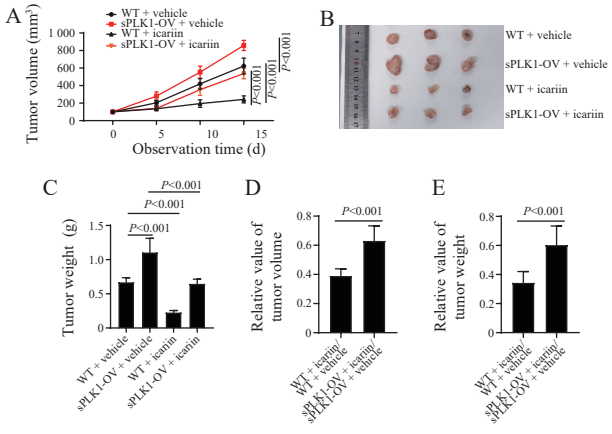

Figure 8 *In vivo* validation of PLK1 as a novel antitumor target of icariin

A, tumor growth curves. B, representative tumor images at study endpoint. C, tumor weight. D, relative values of tumor volume. E, relative values of tumor weight.

4 Discussion

4.1 Hierarchy of target discovery and validation: from multi-target prediction to dominant target identification

Our study began with an unbiased network pharmacology-based prediction, identifying 36 potential targets shared by icariin and HCC. From this candidate pool, PLK1, ABCC1, and MMP3 were prioritized for experimental validation based on objective computational screening: they ranked highest in the RSF algorithm analysis and showed significant associations with HCC patient prognosis in subsequent survival analysis. Their established biological roles in HCC—PLK1 in cell-cycle regulation [27]. ABCC1 in chemoresistance [28] and MMP3 in extracellular matrix degradation [29], provided supporting rationale for their relevance, but the primary driver for their selection was the computational prediction outcome, not a mere repetition of prior findings.

Critically, the “multi-target” prediction required functional prioritization through experimental interrogation. While molecular docking suggested potential binding of icariin to all three targets, subsequent enzymatic inhibition assays and cellular rescue experiments clearly demonstrated that PLK1 acts as the primary and necessary target mediating the anti-proliferative effect of icariin. In contrast, ABCC1 and MMP3, though possibly part of icariin's broader pharmacological network, played secondary roles in the models examined here. This functional stratification—distinguishing the dominant target from subordinate ones—underscores the essential role of experimental validation in translating computational predictions into biologically reliable conclusions, and cautions against equating predicted interactions with equivalent functional importance.

4.2 The central role of the PLK1-FoxM1 axis

Having established PLK1 as the dominant target, we delved into its downstream mechanisms. The study found that icariin specifically reduces the phosphorylation level of PLK1 at Thr210, a key switch for its kinase activity. More mechanistically significant, we discovered for the first time that icariin can disrupt the physical interaction between PLK1 and its key substrate, the transcription factor FoxM1. Our genetic rescue experiment—where knockdown of FoxM1 restored icariin's inhibitory effect on PLK1-overexpressing cells—provides strong evidence that the PLK1-FoxM1 signaling axis is the core downstream pathway through which icariin exerts its effects. FoxM1 has been confirmed as a crucial phosphorylation substrate of PLK1, driving immune escape and metastasis in HCC [26]. This finding of the current study further anchors icariin's mechanism of action to a well-defined oncogenic module, significantly enhancing the precision of its mechanistic explanation and the theoretical basis for its therapeutic targeting.

4.3 Limitations and future perspectives

This study has several limitations. First, the breadth of network pharmacology prediction is constrained by the coverage of the underlying databases. Second, pharmacokinetic properties are a key bottleneck for the druggability of natural products. Although this study demonstrated the efficacy of icariin in cellular and animal models, its oral bioavailability, *in vivo* metabolic pathways, and optimal dosing regimens require systematic investigation, which is essential before advancing it to the preclinical stage. Third, the *in vivo* experiments in this study employed immunodeficient models, precluding an assessment of icariin's impact on the tumor immune microenvironment.

Interestingly, our bioinformatic analysis suggested a correlation between PLK1 expression and the degree of immune cell infiltration in HCC tumors. Combined with the reported roles of PLK1 and FoxM1 in regulating tumor immunity [26], we speculate that icariin, by inhibiting the PLK1-FoxM1 axis, may potentially remodel the immunosuppressive microenvironment. This highly compelling hypothesis urgently awaits validation in future studies using immunocompetent models.

Based on the current findings, future research can be expanded in several directions: (i) combination therapy: explore the combination of icariin with conventional chemotherapeutic agents to reverse drug resistance, leveraging its weak inhibitory effects on ABCC1; (ii) immunomodulatory mechanisms: comprehensively evaluate the impact of icariin on tumor-associated immune cells (e.g., T cells, macrophages) in immunocompetent models; (iii) structural optimization and delivery: design icariin derivatives with enhanced activity and improved pharmacokinetic properties or develop novel delivery systems to increase targeting and efficacy, based on the PLK1 binding mode.

5 Conclusion

This study identifies PLK1 as the primary direct target of icariin against hepatocellular carcinoma and elucidates the molecular mechanism by which it exerts anti-cancer effects through inhibiting PLK1 kinase activity and disrupting the PLK1-FoxM1 interaction. This work not only provides a solid theoretical foundation and a clear target for the anti-HCC application of icariin but also offers an integrative research model for rigorously studying multi-target natural products, spanning from computational prediction to in-depth mechanistic investigation.

Fundings

Linyi Key Research and Development Program (2024YX0044).

Ethical statement

The experimental protocol was approved by the Institutional Animal Care and Use Committee (IACUC) of Beijing Langke Biotechnology Co., Ltd. [Animal Ethic Approval No. IACUC-20230901-01; Facility License No. SYXK (Jing) 2023-0004; Laboratory Animal Use License No. 110324231104736913].

Author contributions

Wei Zhang: formal analysis, investigation, and writing – original draft. Fenglian Ma: investigation. Xiangjun Sun: conceptualization, supervision, and writing – review & editing. All authors approved the submission and take responsibility for this manuscript.

Competing interests

The authors declare no conflict of interest.

References

[1] HAN BF, ZHENG RS, ZENG HM, et al. Cancer incidence and mortality in China, 2022. Journal of the National Cancer Center, 2024, 4(1): 47–53.

[2] MORIS D, MARTININO A, SCHILTZ S, et al. Advances in the treatment of hepatocellular carcinoma: an overview of the current and evolving therapeutic landscape for clinicians. CA, 2025, 75(6): 498–527.

[3] YUE MJ, LIU YL, FENG XA, et al. Epimedii Folium flavonoids: a double-edged sword effect on the liver, a dual exploration of efficacy and toxicity. Journal of Pharmaceutical Analysis, 2025, 15(10): 101269.

[4] GE D, MA SQ, SUN TT, et al. Pulmonary delivery of dual-targeted nanoparticles improves tumor accumulation and cancer cell targeting by restricting macrophage interception in orthotopic lung tumors. Biomaterials, 2025, 315: 122955.

[5] LI ZF, LIU PX, CHEN W, et al. Hypoxia-cleavable and specific targeted nanomedicine delivers epigenetic drugs for enhanced treatment of breast cancer and bone metastasis. Journal of Nanobiotechnology, 2023, 21(1): 221.

[6] YU Z, GUO JF, HU MY, et al. Icaritin exacerbates mitophagy and synergizes with doxorubicin to induce immunogenic cell death in hepatocellular carcinoma. ACS Nano, 2020, 14(4): 4816–4828.

[7] XIAO Y, YAO WX, LIN MZ, et al. Icaritin-loaded PLGA nanoparticles activate immunogenic cell death and facilitate tumor recruitment in mice with gastric cancer. Drug Delivery, 2022, 29(1): 1712–1725.

[8] GU Y, LI ZY, LI H, et al. Exploring the efficacious constituents and underlying mechanisms of Sini Decoction for sepsis treatment through network pharmacology and multi-omics. Phytomedicine, 2024, 123: 155212.

[9] KIM S, CHEN J, CHENG TJ, et al. PubChem 2025 update. Nucleic Acids Research, 2025, 53(D1): D1516–D1525.

[10] JI KY, LIU C, LIU ZQ, et al. Comprehensive assessment of nine target prediction web services: which should we choose for target fishing? Briefings in Bioinformatics, 2023, 24(2): bbad014.

[11] FILATOVA A, REVEGUK I, PIATKOVA M, et al. Annotation of uORFs in the OMIM genes allows to reveal pathogenic variants in 5'UTRs. Nucleic Acids Research, 2023, 51(3): 1229–1244.

[12] BARSHIR R, FISHILEVICH S, INY-STEIN T, et al. GeneCaRNA: a comprehensive gene-centric database of human non-coding RNAs in the GeneCards suite. Journal of Molecular Biology, 2021, 433(11): 166913.

[13] CLOUGH E, BARRETT T, WILHITE SE, et al. NCBI GEO archive for gene expression and epigenomics data sets: 23-year update. Nucleic Acids Research, 2024, 52(D1): D138–D144.

[14] JIA AQ, XU L, WANG Y. Venn diagrams in bioinformatics. Briefings in Bioinformatics, 2021, 22(5): bbab108.

[15] LOSIC B, CRAIG AJ, VILLACORTA-MARTIN C, et al. Intratumoral heterogeneity and clonal evolution in liver cancer. Nature Communications, 2020, 11: 291.

[16] KIM Y, KANG JW, KANG J, et al. Novel deep learning-based survival prediction for oral cancer by analyzing tumor-infiltrating lymphocyte profiles through CIBERSORT. OncoImmunology, 2021, 10(1): 1904573.

[17] CASTANZA AS, RECLA JM, EBY D, et al. Extending support for mouse data in the Molecular Signatures Database (MSigDB). Nature Methods, 2023, 20(11): 1619–1620.

[18] AIBAR S, GONZÁLEZ-BLAS CB, MOERMAN T, et al. SCENIC: single-cell regulatory network inference and clustering. Nature Methods, 2017, 14(11): 1083–1086.

[19] PENG YY, XIAO B, ZHANG MQ. Decoding monocyte signatures in ischemic stroke: a multi-scale transcriptomic approach. Neural Regeneration Research, 2025. doi: 10.4103/NRR.NRR-D-24-01669.

[20] ONO K, FONG D, GAO CZ, et al. Cytoscape Web: bringing network biology to the browser. Nucleic Acids Research, 2025, 53(W1): W203–W212.

[21] JIAO ZL, GAO XM. Potential targets and mechanisms of Guarana in the treatment of Alzheimer's disease based on network pharmacology. Digital Chinese Medicine, 2023, 6(1): 55–66.

[22] SILBERMANN K, STEFAN SM, ELSHAWADFY R, et al. Identification of thienopyrimidine scaffold as an inhibitor of the ABC transport protein ABCC1 (MRP1) and related transporters

using a combined virtual screening approach. Journal of Medicinal Chemistry, 2019, 62(9): 4383–4400.

[23] OH Y, JUNG H, KIM H, et al. Design and synthesis of a novel PLK1 inhibitor scaffold using a hybridized 3D-QSAR model. International Journal of Molecular Sciences, 2021, 22(8): 3865.

[24] WANG D, LIN YK, XU FH, et al. SIRPα maintains macrophage homeostasis by interacting with PTK2B kinase in *Mycobacterium tuberculosis* infection and through autophagy and necroptosis. EBioMedicine, 2022, 85: 104278.

[25] GAO SC, ZHANG WY, DAI JH, et al. Icariin mediates autophagy and apoptosis of hepatocellular carcinoma cells induced by the β-catenin signaling pathway through lncRNA LOXL1-AS1. Naunyn-Schmiedeberg's Archives of Pharmacology, 2025, 398(7): 8455–8468.

[26] XU R, LEE YJ, KIM CH, et al. Invasive FoxM1 phosphorylated by PLK1 induces the polarization of tumor-associated macrophages to promote immune escape and metastasis, amplified by IFITM1. Journal of Experimental & Clinical Cancer Research, 2023, 42(1): 302.

[27] CHANG YS, SU CW, CHEN SC, et al. Upregulation of USP22 and ABCC1 during sorafenib treatment of hepatocellular carcinoma contribute to development of resistance. Cells, 2022, 11(4): 634.

[28] HAN YH, WANG YQ, BO JQ, et al. ABCC1 is a predictive biomarker for prognosis and therapy in hepatocellular carcinoma. European Review for Medical and Pharmacological Sciences, 2023, 27(8): 3597–3611.

[29] HASSAN HM, HAMDAN AM, ALATTAR A, et al. Evaluating anticancer activity of emodin by enhancing antioxidant activities and affecting PKC/ADAMTS4 pathway in thioacetamide-induced hepatocellular carcinoma in rats. Redox Report, 2024, 29(1): 2365590.

(Editor-in-Charge Siyi Wei)

整合网络药理学与实验验证探究淫羊藿素靶向 PLK1 抑制肝细胞癌的作用机制

张伟[a], 马丰连[a], 孙象军[b*]

a. 广州中医药大学临沂市人民医院研究生培养基地, 山东 临沂 276003, 中国
b. 临沂市人民医院肝胆外科, 山东 临沂 276003, 中国

【摘要】目的 整合网络药理学与实验验证，系统阐明淫羊藿素抗肝细胞癌（HCC）的分子机制及其核心作用靶点。**方法** 基于 PubChem 和 SwissTargetPrediction 数据库筛选淫羊藿素潜在靶点，结合癌症基因组图谱（TCGA）与基因表达综合数据库（GEO）中的 HCC 相关基因进行交集分析。通过基因本体（GO）富集和京都基因与基因组百科全书（KEGG）通路分析明确候选靶点的生物学功能。采用随机生存森林算法筛选关键基因，并通过免疫浸润分析评估其与肿瘤微环境的关系。应用分子对接预测淫羊藿素与核心靶点的结合能力，并通过体外酶活抑制实验验证。在 HepG2 细胞中通过过表达实验确定功能性靶点，运用蛋白质印迹和免疫共沉淀技术探究作用机制。通过建立皮下 HepG2 异种移植小鼠模型，监测肿瘤体积变化及终点肿瘤重量以评估体内抗肿瘤疗效，并分析 Polo 样激酶 1（PLK1）过表达对淫羊藿苷介导的肿瘤生长抑制作用的影响。**结果** 网络药理学分析鉴定出淫羊藿素与 HCC 的 36 个共同靶点，主要富集于低氧诱导因子-1（HIF-1）、磷脂酰肌醇-3-激酶/蛋白激酶 B（PI3K/AKT）与叉头框蛋白 O（FoxO）等信号通路。其中，*PLK1*、ATP 结合盒转运蛋白 C 亚家族成员 1（*ABCC1*）和基质金属蛋白酶 3（*MMP3*）被确定为关键基因，其高表达均与患者不良预后显著相关（分别为 $P < 0.0001$、$P = 0.004$、$P = 0.03$）。免疫浸润分析提示这三个基因与多种免疫细胞显著相关，可能参与调控肿瘤免疫微环境。分子对接预测淫羊藿素可与上述靶点稳定结合，体外酶活实验证实淫羊藿素（20 μmol/L）对 PLK1 的抑制率最高（49.67% ± 4.19%），显著高于 ABCC1（24.33% ± 3.40%）和 MMP3（38.00% ± 3.06%）。功能验证表明，PLK1 过表达可逆转淫羊藿素对 HepG2 细胞增殖的抑制作用（$P < 0.05$），而 ABCC1 或 MMP3 过表达无此效应，提示 PLK1 是淫羊藿素的主要功能靶点。机制研究发现淫羊藿素特异性降低 PLK1 的磷酸化水平并破坏其与叉头框蛋白 M1（FoxM1）的相互作用。体内实验证实 PLK1 过表达可显著削弱淫羊藿素对荷瘤小鼠肿瘤生长的抑制作用（$P < 0.001$）。**结论** PLK1 是淫羊藿素抗 HCC 作用的关键靶点，其机制与抑制 PLK1-FoxM1 轴有关，为淫羊藿素的临床转化应用提供了理论依据。

【关键词】淫羊藿素；肝细胞癌；Polo 样激酶 1（PLK1）；磷酸化；分子对接